Opto-Electronics Review 28 (2020) 82-92

PAN POLISH ACADEMY OF SCIENCES

Opto-Electronics Review

journal homepage: http://journals.pan.pl/opelre

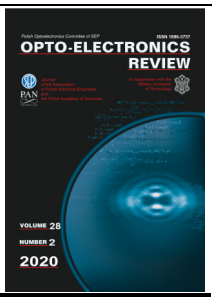

Comparison of performance limits of HOT HgCdTe photodiodes with 2D material infrared photodetectors

A. Rogalski[a], M. Kopytko[b*], P. Martyniuk[a], W. Hu[b]

[a] Institute of Applied Physics, Military University of Technology, 2 Kaliskiego St., 00-908 Warsaw, Poland
[b] State Key Laboratory of Infrared Physics, Shanghai Institute of Technical Physics, Chinese Academy of Sciences, 500 Yu Tian Road, Shanghai 200083, China

Article info

Article history:
Received 24 Mar. 2020
Received in revised form 08 Apr. 2020
Accepted 08 Apr. 2020

Keywords:
2D material photodetectors,
HOT infrared detectors,
HgCdTe photodiodes, p-i-n depleted photodiodes, BLIP performance

Abstract

The semiempirical rule, "Rule 07" specified in 2007 for P-on-n HgCdTe photodiodes has become widely popular within infrared community as a reference for other technologies, notably for III-V barrier photodetectors and type-II superlattice photodiodes. However, in the last decade in several papers it has been shown that the measured dark current density of HgCdTe photodiodes is considerably lower than predicted by benchmark Rule 07. Our theoretical estimates carried out in this paper support experimental data.

Graphene and other 2D materials, due to their extraordinary and unusual electronic and optical properties, are promising candidates for high-operating temperature infrared photodetectors. In the paper their room-temperature performance is compared with that estimated for depleted P-i-N HgCdTe photodiodes. Two important conclusions result from our considerations: the first one, the performance of 2D materials is lower in comparison with traditional detectors existing on global market (InGaAs, HgCdTe and type- II superlattices), and the second one, the presented estimates provide further encouragement for achieving low-cost and high performance HgCdTe focal plane arrays operating in high-operating temperature conditions.

1. Introduction

Infrared (IR) detector technology tracks their origin back to February 11, 1800, when John Frederik William Herschel has used a thermometer to detect invisible to the human eye rays refracted in the prism. Initially IR detection systems were based on thermal detectors: thermometers, thermocouples, and bolometers. The development of IR photon detector technology was begun around 1930 with the appearance of photo-emissive photocathodes and lead salt photoconductors. World War II initiated their wider development. Lead sulphide photoconductors were introduced to the manufacturing stage in Germany in about 1943. However, the invention of a transistor on December 23, 1947 at Bell Laboratories in Murray Hill, New Jersey, by William Shockley, John Bardeen and Walter Brattain gave the development possibilities of modern detection systems (see Fig. 1). Photon detectors based on Ge, Si, InSb and HgCdTe appeared in the next decade. In 1956, Texas Instruments began research on IR technology which led to the signing of several contracts with a linear scanner and, subsequently, to the invention of the first forward-looking infrared (FLIR) camera in 1963. Next, in 1972 Texas Instruments also invented the Common Module concept, which contributed to a significant cost reduction and allowed for reuse of common components. These systems belong to the, so-called, first generation scanning systems. HgCdTe has inspired development of the next three "generations" of detector devices shortly described in the Fig. 1 caption which found mainly military but also civilian applications. The emergence of advanced epitaxial techniques [molecular beam epitaxy (MBE) and metalorganic chemical vapour deposition (MOCVD)] combined with the photolithography process revolutio-

* Corresponding author: e-mail malgorzata.kopytko@wat.edu.pl

https://doi.org/10.24425/opelre.2020.132504

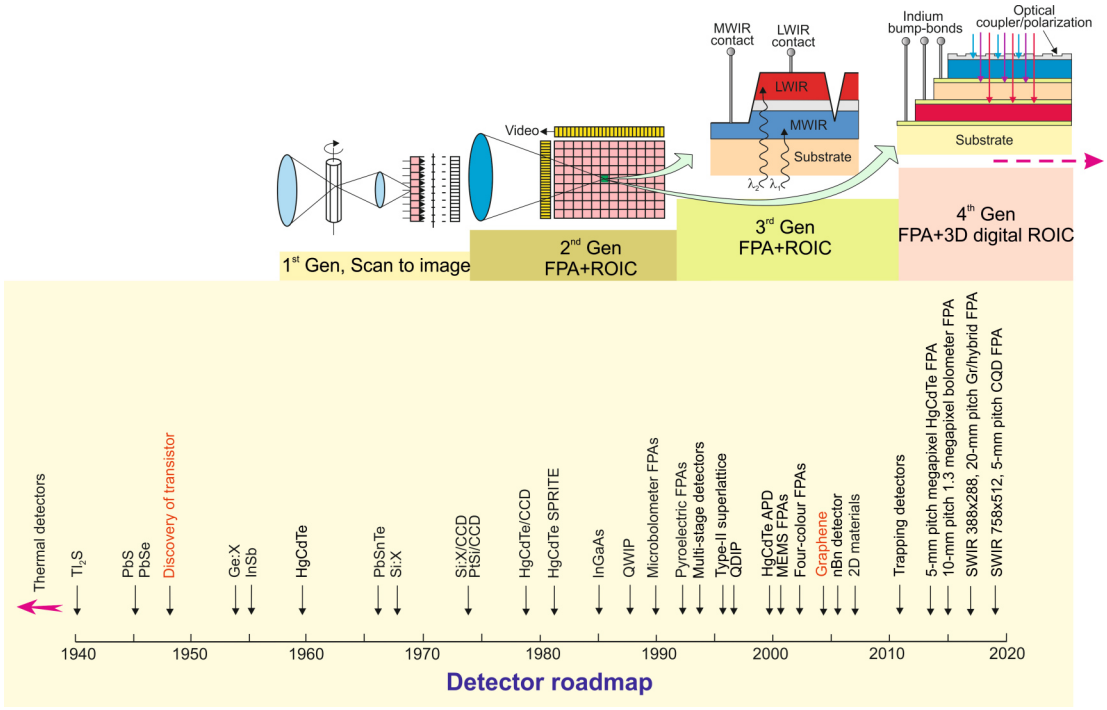

Fig. 1. The history of development of IR detectors and imaging systems.. For principal military and civilian applications four generation systems can be considered: first generation (scanning systems), second generation (staring systems - electronically scanned), third generation (staring systems with large number of pixels and two-colour functionality), and fourth generation (staring systems with very large number of pixels, multi-colour functionality, 3D ROIC, and other on-chip functions; e.g., better radiation/pixel coupling, avalanche multiplication in pixels, polarization/phase sensitivity).

nized the IR detector systems industry enabling the design and fabrication of complex focal plane arrays (FPAs). The first three generations of imaging devices systems primarily rely on planar FPAs. We are currently dealing with the fourth generation staring systems, which the main features are to be: high resolution (with a very large number of pixels – above 108), multi-colour functionality, three dimensional readout integration circuits (3D ROIC), and other integration functions; e.g., better radiation/pixel coupling, avalanche multiplication in pixels, polarization/phase sensitivity. Evolution of the fourth generation is inspired by the most famous visual systems which are the biological eyes. Solution based on the Petzval-matched curvature allowing reduction of field curvature aberration, eq. bonding detectors to flexible or curved molds, has been proposed [1]. In addition, it combines such advantages as simplified lens system, electronic eye systems and wide field-of-view [2,3]. The colloidal quantum dot (CQD) [4] and 2D layered material [5] photodetectors fabricated on flexible substrates are promising materials to overcome technical challenges in fourth generation IR systems' development.

Graphene was the first modern 2D material to be isolated in 2004 [6]. Since then, there have been literally hundreds of other examples [7]. Nowadays, due to infancy stage of technology, the performance of 2D material HOT photodetectors is lower in comparison with traditional detectors existing on global market based on InGaAs, HgCdTe and type-II superlattices (T2SLs) [8,9]. Independently of that, it is interesting to compare the performance of 2D material photodetectors with a fundamental limitation of HgCdTe photodiodes.

At present stage of HgCdTe technology, the semi-empirical rule, "Rule 07" (specified in 2007 [10]) is not a good approach for prediction of HgCdTe detector and system performance. This benchmark is merely a photodiode manifestation with an active n-type region in a P-on-n structure (doping concentration of about 10^{15} cm^{-3}) limited by Auger's 1 diffusion current. If photodiode performance is limited by a p-type diffusion current or by depletion current, Rule 07 is not a suitable estimation. Since 2007, the n-type doping in active region of P-on-n has been decreased almost two orders of magnitude and in Teledyne growth HgCdTe epilayers by MBE achieve 10^{13} cm^{-3}.

In several papers it has been shown that the depleted background limited HgCdTe photodiodes can achieve the level of room-temperature dark current considerably lower than predicted by Rule 07 [11,12]. For those reasons, in the present paper, the performance of high-operating temperature (HOT) 2D material photodetectors is compared with that predicted for depleted P-i-N HgCdTe photodiodes. Theoretical estimates are collated with experimental data for both HgCdTe photodiodes and 2D layered detectors.

2. Trends in development of IR HOT photodetectors

In 1999 the famous British scientist Tom Elliott and his co-workers wrote *that there is no fundamental obstacle to obtaining room temperature operation of photon detectors at room temperature with background-limited performance even in reduced fields of view* [13]. The invention of a microbolometer array was a milestone step in development of infrared cameras operating at room temperature. However, microbolometer belongs to the class of thermal detectors with limited response time – typically in the millisecond range. In order to omit this limitation, further efforts are directed to increase operating temperature of photon detectors.

The present efforts in IR detector technology are particularly addressed to reduction of a system's cost by a decrease of the imaging systems size, weight, and power consumption (SWaP). This also leads to an increase of the operating temperature [14,15]. The ultimate goal is the fabrication of HOT photodetectors characterized by the dark current less than the system background flux current and with the 1/*f* noise negligible small in comparison to the shot noise of the background flux.

In several papers it was shown that the detector size, *d*, and *F*-number (*f*/#) are basic parameters of IR systems [16,17]. Since they depend on $F\lambda/d$ (where λ is the wavelength), these parameters have a great impact on the detection range, as well as the noise equivalent difference temperature (*NEDT*) [17]:

$$Range = \frac{D\Delta x}{M\lambda}\left(\frac{F\lambda}{d}\right), \tag{1}$$

$$NEDT \approx \frac{2}{C\lambda\left(\eta\Phi_B^{2\pi}\tau_{int}\right)}\left(\frac{F\lambda}{d}\right). \tag{2}$$

Here, *D* is the aperture, *M* is the number of pixels required to identify the target Δx, *C* is the scene contrast, η is the detector collection efficiency, $\Phi_B^{2\pi}$ is the background flux into a 2π FOV, and τ_{int} is the integration time. As follows from Eqs. (1) and (2), the parameter space defined by $F\lambda$ and *d* may be used in the optimal design of any IR system. As is shown in Ref. 18, for IR system with *f*/1 optics, the smallest usable detector size should be 2 μm and 5 μm for the mid- wave infrared (MWIR) and long-wave infrared (LWIR) range, respectively. With more realistic *f*/1.2 optics, the smallest usable detector size is of 3 μm in the MWIR and of 6 μm in the LWIR.

It is well known and can be repeated after Kinch [17] that: *the ultimate cost reduction for an IR system will only be achieved by the room temperature operation of depletion-current limited arrays with pixel densities that are fully consistent with background and diffraction-limited performance due to the system optics.* The depletion-current limited P-i-N photodiodes demand long Shockley-Read-Hall (SRH) carrier lifetime, τ_{SRH}, to meet the requirements of a low dark current. The long SRH lifetime of HgCdTe makes this material a great candidate for room-temperature operation [17].

The SRH generation-recombination mechanism in HgCdTe is associated with residual impurities and native defects. Based on the data collected by Kinch *et al.* in 2005 [19], the measured values of SRH lifetimes for the LWIR n-type HgCdTe range from 2 up to 20 μs at 77 K regardless of doping concentration for values bellow 10^{15} cm^{-3}. The SRH lifetimes for MWIR material are typically slightly longer, in the range from 2 to 60 μs. However, the recent data show the values of τ_{SRH} considerably larger in a low temperature range and low doping concentrations, above 200 μs up to even 50 ms depending on the cut-off wavelength [17] – see Table 1. Recently published paper by Gravrand *et al.* [20] has shown that the estimated SRH carrier lifetimes, obtained from direct measurements (photoconductive or photoluminescence decay), as well as indirect estimations from current-voltage (*I-V*) characteristics for most tested MWIR photodiodes from Leti and Sofradir, are in the range between 10 and 100 μs. These values are lower than previously estimated by US research groups. However, they were estimated for photodiodes with higher doping in active region – of above 10^{14} cm^{-3}, while the range of low doping that is reproducibly generated in Teledyne growth HgCdTe epilayers by MBE is of about 1013 cm^{-3}. Moreover, in a just published announcement result, that Teledyne has confirmed fabrication of the depletion layer limited P-i-N HgCdTe photodiodes with SRH recombination centres having lifetimes in the range from 0.5 to 10 ms [21].

Table 1
Summary of the SRH carrier lifetimes determined on the basis of *I-V* and FPA characteristics (after Ref. 17).

	x composition	τ_{SRH} (μs)
LWIR	0.225	> 100 at 60 K
MWIR	0.30	> 1000 at 110 K
	0.30	~ 50000 at 89 K
SWIR	0.455	> 3000 at 180 K

P-i-N heterostructure photodiode is shown in Fig. 2(a) [10]. The active region consists of an undoped i-region (ν region, low n-doping) sandwiched between the wider bandgap cap (P) and the buffer (N) region. The surrounded

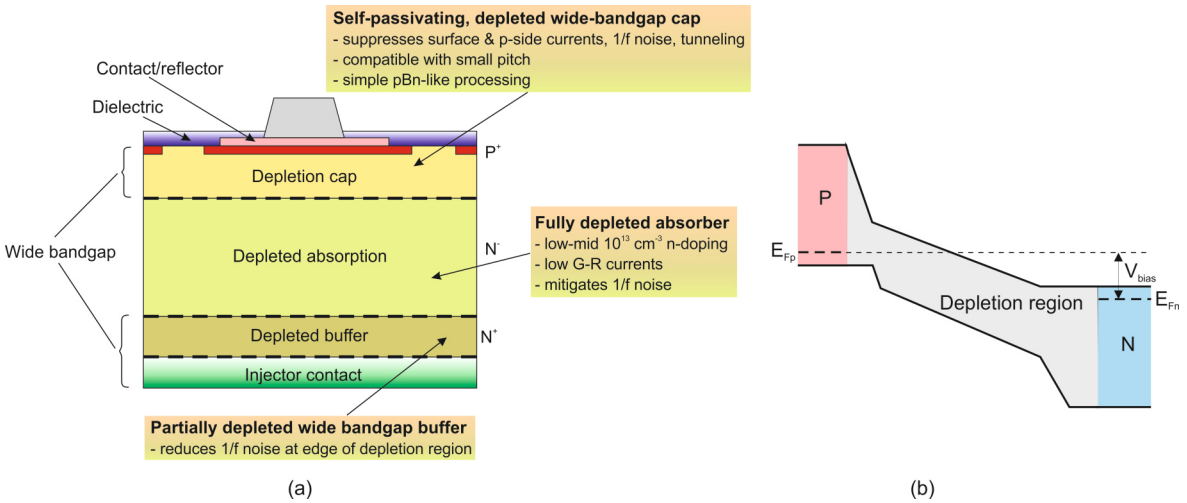

Fig. 2. P-i-N photodiode: (a) energy band diagram under reverse bias, (b) heterojunction architecture (adapted after Ref. 11).

wide- gap contact layers are designed to suppress the dark current generation from these regions and to reduce tunnelling current, as well as $1/f$ and random telegraph noise. Very low doping in the absorber region (below 5×10^{13} cm^{-3}) is required to allow for a full depletion at zero or a low value of reverse bias [see Fig. 2(b)]. The choice of absorber thickness should be a trade-off between response speed and quantum efficiency (or responsivity). To achieve short response times, the absorber thickness should be small and fully depleted. For high quantum efficiency the absorption region should be thick enough to effectively collect photogenerated carriers. However, to enhance quantum efficiency while maintaining high response speed, an external resonant microcavity has been proposed. In this approach, the absorber is placed inside a cavity, so that a large portion of photons can be absorbed even with a small detection volume. The fully-depleted P-i-N structure is compatible with a small pixel size, meeting the low crosstalk thanks to the vertical electric field [10,17].

The limiting dark currents in a fully depleted P-i-N photodiode come from diffusion current in N and P regions (depending on SRH and Auger generations) and depletion current ruled by SRH generation in the space charge region. If P-i-N photodiode operates under reverse bias, Auger suppression effect is occurring. This effect is important in HOT condition when the intrinsic carrier concentration is much larger than the dopant concentration ($n_i >> N_{dop}$). In non-equilibrium, a large number of intrinsic carriers can be swept-out the absorber region down to the doping level. It is expected that this impact is larger for lower n-doping levels since n_i is proportionally higher. At a very low level of n-type doping (about 10^{13} cm^{-3}) the ultimate performance of a P-i-N photodiode is limited by SRH recombination and neither Auger recombination nor Auger suppression (see section 3.2). Influence of the radiative recombination is still debatable but is not considered as a limiting factor of small pixel HgCdTe photodiodes. Moreover, due to the photon recycling effect, the radiative recombination influence can be significantly reduced [12].

3. Analysis of photodetector structures and discussion

3.1 2D material photodetectors: current responsivity vs. response time

The current responsivity of the photodetector is equal to

$$R_i = \frac{\lambda\eta}{hc} qg, \tag{3}$$

where λ is the wavelength, η is the quantum efficiency, h is the Planck constant, c is the velocity of light, q is the electron charge, and g is the photoelectrical gain. The quantum efficiency can be understood as the number of electron-hole pairs generated by one incident photon and describes how well the detector is coupled to the impinging radiation. The photoelectrical gain is the number of carriers passing contacts per one generated electron-hole pair and describes how well the generated charge carriers are used to generate a photodetector current response.

In general, the photoconductive gain can be defined as:

$$g = \frac{\tau}{t_t}, \tag{4}$$

where τ is the carrier lifetime and t_t is the transit time of electrons between ohmic contacts. In other words, the photoconductive gain is given by the ratio of free carrier lifetime to transit time between device electrodes. Depending on whether the drift length, $L_d = v_d\tau$, is less than or greater than the distance between the electrodes, l, the photoconductive gain can be smaller or larger than one. If $L_d > l$, a free charge carrier swept out at one electrode is immediately replaced by an equivalent free charge carrier injected by the opposite electrode. Therefore, the free carrier will continue to circulate until it recombines what gives the value of $g > 1$.

In the case of the photodiode, the photoelectric gain is usually equal to 1, due to the separation of minority carriers by the depletion region electrical field. However, in a hybrid combination of 2D material photodetectors, photosensitization and carrier transport take place in separately optimized regions: one for efficient light absorption and the second to provide fast charge reticulation. In this way, ultra-high gain up to 10^8 electrons per photon and exceptional responsivities for short wavelength infrared (SWIR) photodetectors have been demonstrated [22].

The simple architecture of a hybrid phototransistor, very popular in design of 2D material photodetectors with the fast transfer channel for charge carriers, is shown in Fig. 3. Reduction of thickness of 2D materials to an individual atomic layer makes it more susceptible to local electric fields than conventional bulk materials and the photogating effect can strongly modulate the channel conductivity by the external gate voltage, V_g. Improving the optical gain is particularly important since the quantum efficiency is limited because of the weak absorption in 2D materials. This effect is especially seen in a longer wavelength IR spectral region where the light absorption is weak. In the case of a hybrid detector shown in Fig. 3(a), the holes are injected into a transporting channel, whereas electrons remain in the photoactive layer. The injected charges can reticulate even several thousand times before recombination, giving contribution in gain under illumination. The photocarrier lifetime is enhanced through both bandgap structure and defect engineering, and at the same time the trapping mechanisms limit the photodetector's response time even to several seconds.

The photocurrent change by photogating effect can be written as [23]:

$$I_{ph} = g_m \Delta V_G, \tag{5}$$

where g_m is the transconductance and ΔV_g is the equivalent photoinduced voltage. Figure 3(d) indicates a shift of the $I_{ds}(V_G)$ trace after the light illumination. Generally, both positive and negative photoconductance behaviours are observed in hybrid 2D structures and operating points A and B, related to g_m and ΔV_g, perform opposite directions.

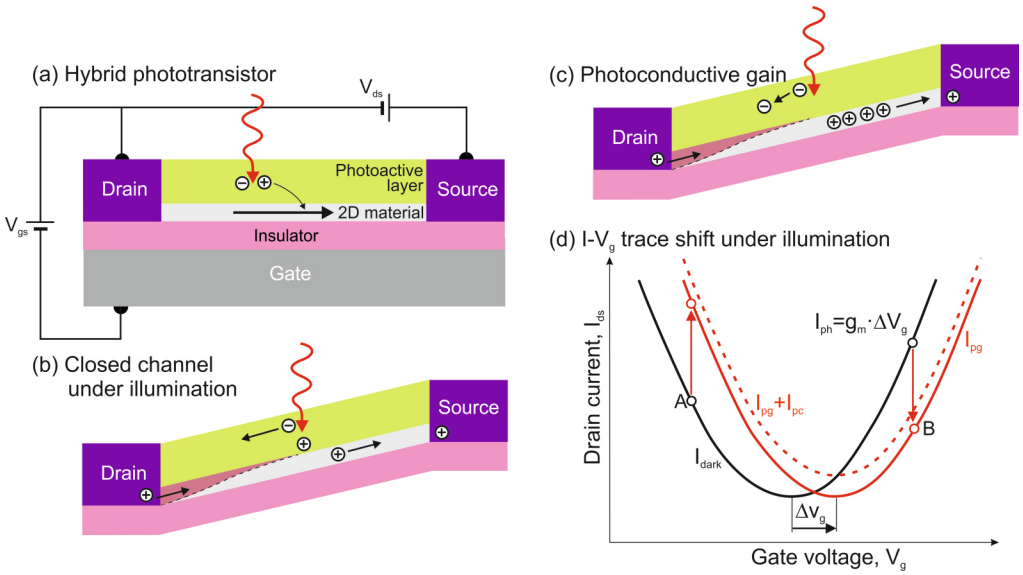

Fig. 3. Photogating effect in 2D material photodetectors: (a) the operation of hybrid phototransistor, (b) closed channel under illumination, (c) photoconductive gain, and (d) *I-V*$_G$ trace under illumination.

Figure 4 shows the spectral responsivity of graphene-based photodetectors designed for visible and near-infrared (NIR) spectral ranges compared to the silicon and InGaAs devices commercially available in the market [22,24-32]. The highest current responsivity, above 10^7 A/W has been achieved for hybrid Gr/quantum dot (QD) photodetectors with enhancement trapped charge lifetimes. As is shown, the high mobility of graphene combined with the enhanced lifetimes of trapped charge in the quantum dots provide a photodetector responsivity up to seven orders of magnitude higher in comparison with standard bulk photodiodes, where $g \approx 1$. Higher responsivity of a Si avalanche photodiode (APD), up to 100 A/W, is caused by avalanche process. High responsivity gives the opportunity to design devices suitable to detect low level signals. Nevertheless, the very slow frequency response of 2D material photodetectors (< 10 Hz) being the result of the long lifetime of the traps considerably limits real detector functions.

It is interesting to emphasize the exceptional electrical and optical properties of gold patched graphene nanostripe photodetectors presented by Cakmakyapan *et al*. [32]. The photodetector is characterized with an ultra-wide spectral range from visible to IR radiation with a high responsivity values ranging from 0.6 A/W for the wavelength of 800 nm to 11.65 A/W for 20 μm and operation speed exceeding 50 GHz. As is shown in Fig. 4, its current responsivity (black circles) coincides well with the curve (black line) theoretically predicted for an ideal photodiode in a NIR spectral range.

2D materials show potentials for operation in the wide spectral range from UV to THz, although most of them cover visible and SWIR ranges – see Fig. 5. Similarly, for

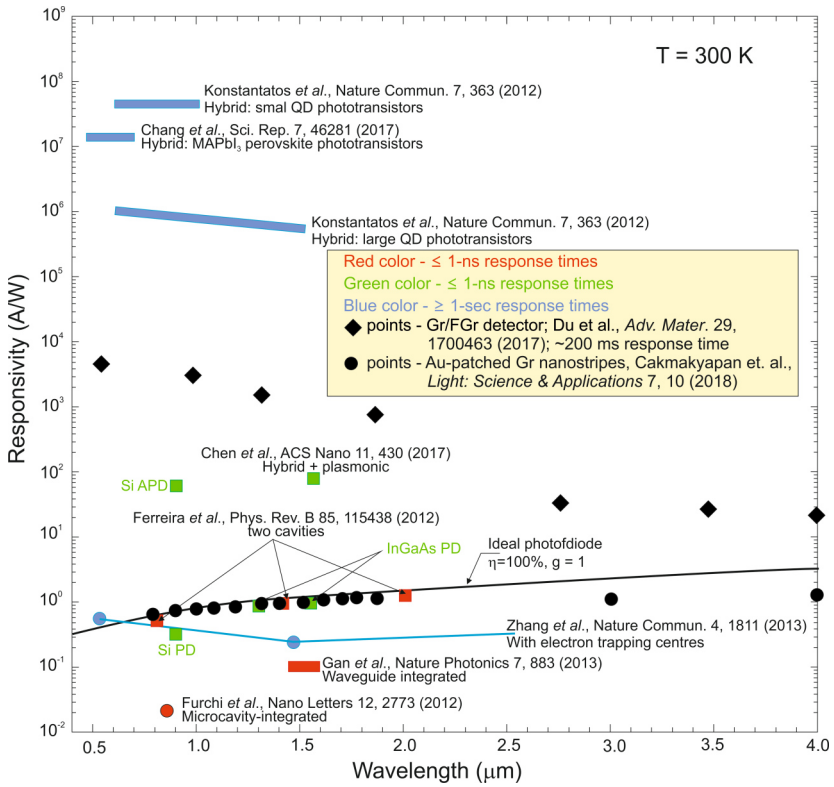

Fig. 4. Room-temperature spectral responsivity of graphene-based photodetectors compared with commercial ones. Black line shows spectral responsivity for ideal photodiode with 100% quantum efficiency and $g = 1$. Red and green colours denote ≤ 1 ns response times, while the blue colour denotes ≥ 1 second response times. The graphene photodetectors are labelled with their reference as well as a brief description of the photodetector style. The commercial photodiodes are shown in green [after Refs. 24-33].

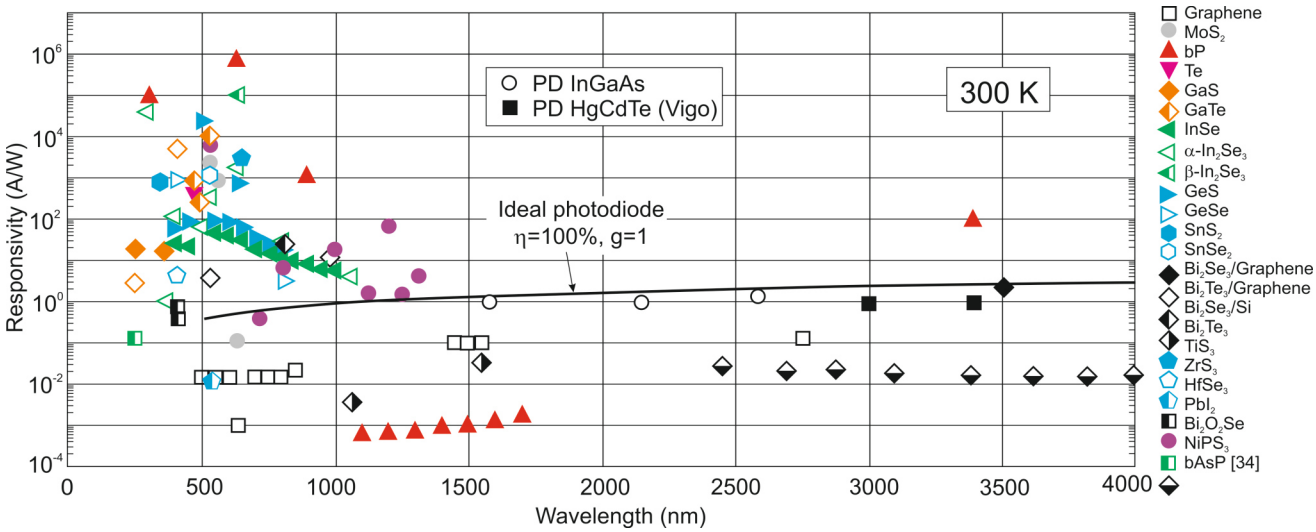

Fig. 5. Summary of spectral responsivities to the layered 2D material photodetectors at room temperature (after Refs. 33 and 34). Black line shows spectral responsivity for ideal photodiode with 100% quantum efficiency and $g = 1$. For comparative goals, the responsivities of commercially available photodetectors (InGaAs and HgCdTe photodiodes) are marked.

graphene photodetectors both high responsivity and short response time cannot be obtained simultaneously in many 2D material-based photodetectors.

Development of pristine 2D material high sensitivity photodetectors depends on e two major challenges: low optical absorption in a thin active region (~ 100 – 200 nm) and short lifetime of photogenerated carriers. In consequence, the trade-off between high responsivity and ultrafast response time in a broadband operation must be found. Photodetectors based on 2D materials display a large variation in their current responsivity and response time [35,36] – about 9 orders of magnitudes as is shown in Fig. 6. To enhance the IR absorption, multiple layers, instead of a single layer, are chosen. In photogating effect photodetectors, 2D materials are used as the fast transfer channel for charge carriers. However, as is mentioned above, their overall disadvantage is a very slow response time (even up to 10^4 ms) due to traps and high capacitance. Typical values are longer than ~10^{-2} ms, what indicates a considerably longer response time in comparison with commercial silicon, InGaAs, and HgCdTe photodiodes; for HOT photodiodes, the response time is typically between 1 and 10 ns. The upper left blank region of Fig. 6(a) confirms the lack of photodetectors that shows both ultra-fast response speed and ultra-high responsivity. Figure 6(b) summarizes the responsivity and response time of different 2D material photodetectors. It is shown that black phosphorus is a good candidate for a fast detection and falls into a region between graphene and TMDs.

3.2 *P-i-N HgCdTe photodiodes*

The diffusion current of a P-i-N HgCdTe photodiode structure arises from the thermal generation of carriers in a thick, un-depleted absorber and is dependent on the Auger and SRH generation in an n-type semiconductor [17]:

$$J_{dif} = \frac{qn_i^2 t_{dif}}{n}\left(\frac{1}{\tau_{A1}} + \frac{1}{\tau_{SRH}}\right), \qquad (6)$$

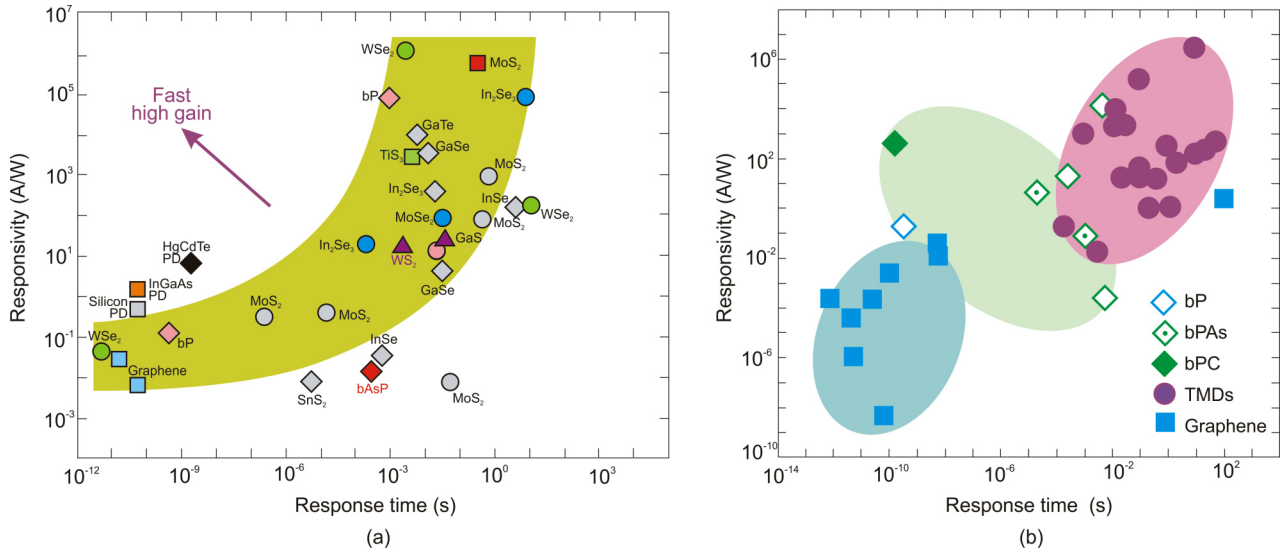

Fig. 6. Responsivity *vs.* response time for 2D material HOT photodetectors: (a) in comparison with commercial silicon, InGaAs and HgCdTe photodiodes (after Ref. 36), and (b) for different types of materials - graphene-based, black phosphorus (bP) and transition metal dichalcogenides (TMDs) (after Ref. 37)

where q stands for the electron charge, n is the electron concentration, t_{dif} is the diffusion region thickness, n_i is the intrinsic carrier concentration, τ_{A1} is the Auger 1 lifetime, and τ_{SRH} is the SRH lifetime. Auger 1 lifetime is related to the hole, electron, and intrinsic carrier concentrations, and τ_{A1} is given by equation:

$$\tau_{A1} = \frac{2\tau_{A1}^{i} n_i^2}{n(n+p)}, \tag{7}$$

where p is the hole concentration and τ_{Ai} is the intrinsic Auger 1 lifetime. For a low temperature operation or a non-equilibrium active volume, when the majority carrier concentration is held equal to the majority carrier doping level [and intrinsically generated majority carriers are excluded ($p << n \approx N_{dop}$)], Eq. (4) becomes:

$$\tau_{A1} = \frac{2\tau_{A1}^{i} n_i^2}{n^2}. \tag{8}$$

The shortest SRH lifetime occurs through centres located approximately at the intrinsic energy level in the semiconductor bandgap. Then, for the field-free region in an n volume ($n >> p$), τ_{SRH} is given by:

$$\tau_{SRH} = \frac{\tau_{no} n_i + \tau_{po}(n+n_i)}{n}, \tag{9}$$

where τ_{no} and τ_{po} are the specific SRH lifetimes. At low temperatures, where $n > n_i$, we have $\tau_{SRH} \approx \tau_{po}$. At high temperatures where $n \approx n_i$, we have $\tau_{SRH} \approx \tau_{no} + \tau_{po}$. For a non-equilibrium active volume, $\tau_{SRH} \approx (\tau_{no} + \tau_{po})n_i/n$ exhibits a temperature dependence given by n_i.

The second component is the depletion current arising from the portion of the absorber that becomes depleted. The depletion current density can be estimated by the following expression:

$$J_{dep} = \frac{q n_i t_{dep}}{\tau_{no} + \tau_{po}}, \tag{10}$$

where t_{dep} is the width of depletion region.

All SRH lifetimes estimated for HgCdTe are usually carried out for a temperature below 300 K. Their extrapolation to 300 K in order to predict the photodiode operation behaviour is questionable. In our estimates we assume τ_{SRH} equal 1 ms, which is supported by experimental data achieved by DRS and Teledyne research groups.

The P-i-N HOT photodiode is characterized by useful properties at reverse bias operation. Figure 7 shows the calculated reverse bias voltage which is required to completely deplete a 5 μm - thick absorber doped at different doping level. For the Rule 7 the doping range of about 10^{15} cm^{-3}, a 5 μm - thick absorber can be fully depleted by applying a relatively high reverse bias between 10 V and 30 V. On the other hand, for the range of doping reached presently at Teledyne (about 10^{13} cm^{-3}), the 5 μm - thick absorber can be fully depleted for a reverse bias from zero up to 0.4 V.

The comparison of diffusion and depletion dark current components *vs.* temperature for MWIR (λ_c = 5 μm) P-i-N photodiode, with the value of SRH carrier lifetime of 1 ms,

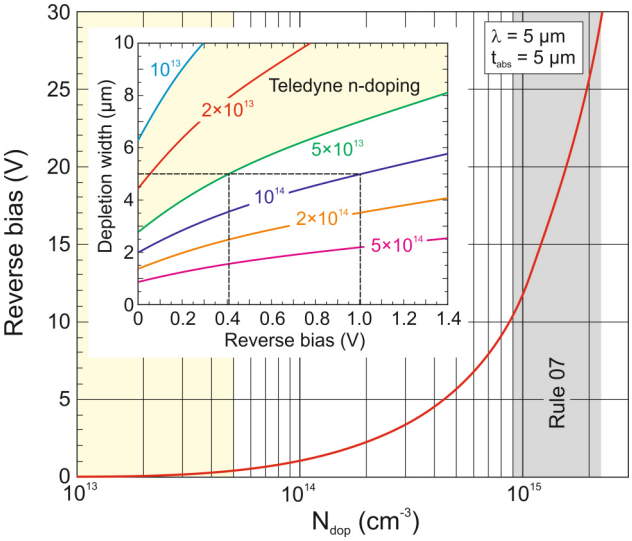

Fig. 7. Calculated reverse bias voltage *vs.* doping concentration required to deplete a 5-μm-thick MWIR HgCdTe absorber. Inset: Width of absorber depletion versus reverse bias voltage and doping concentration.

absorber thickness of 5 μm and doping of 5×10^{13} cm^{-3} is presented in Fig. 8. The diffusion component associated with Auger 1 mechanism is eliminated because of the absence of majority carriers due to exclusion and extraction effects [38,39]. The background radiation calculated from f/3 optics has decisive influence on dark current. It should be mentioned here that the background flux current is defined by the total flux through the optics (limited by f/#) plus the flux from the cold shield. This effect is shown by increasing influence of the background limited performance (BLIP) (f/3) on dark current at temperature above 220 K.

As is shown in Fig. 8, the Teledyne Judson experimentally measured current densities [40], at the bias of -0.3 V, are close to BLIP (f/3) curve – they are located less than one order of magnitude above this limit. The current density at room temperature is even lower than

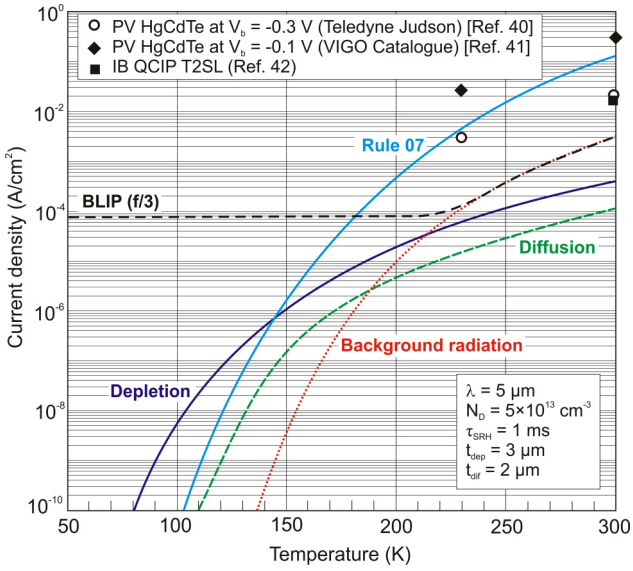

Fig. 8. Detectivity *vs.* temperature for MWIR P-i-N photodiode with the value of τ_{SRH} = 1 ms and absorber doping level of 5×10^{13} cm^{-3}. Thickness of active region is t = 5 μm and consists of t_{dif} = 2 μm and t_{dep} = 3 μm. The experimental data are taken with different sources as marked. PC – photoconductor, PV – photodiode, IB QCIP - interband quantum cascade infrared photo-detector.

predicted by Rule 07. The measured current densities presented by VIGO [41] are about one order of magnitude higher, however in this case they were measured at lower reverse bias, -0.1 V with less effective Auger suppression contribution. It is interesting to notice, that the performance of inter-band quantum cascade infrared photodetectors (IB QCIP) based on T2SLs fabricated with InAs/GaSb coincides very well with the upper experimental data for HgCdTe photodiodes at room temperature [42].

The photodiode D^* is specified based on the current responsivity R_i and the noise current i_n, and can be written as:

$$D^* = \frac{R_i}{i_n}. \tag{11}$$

For the non-equilibrium devices, the i_n value can be calculated including thermal Johnson-Nyquist and shot noises using the following expression:

$$i_n = \sqrt{\frac{4k_BT}{R_dA} + 2qJ_{dark}}, \tag{12}$$

where k_B is the Boltzmann constant, R_dA is the dynamic resistance area product, J_{dark} is the dark current density.

Figure 9 shows calculated detectivity *vs*. temperature for MWIR P-i-N HgCdTe photodiode assuming identical parameters as taken in calculation presented in Fig. 8 (λ_c = 5 μm, τ_{SRH} = 1 ms, t = 5 μm, N_{dop} = 5×10^{13} cm^{-3}). The current responsivity was calculated assuming QE = 1 (however typical QE reaches the reasonable value of about 0.7). As is shown, for an MWIR photodiode with a 5-μm cut-off wavelength and low doping in active region, D^* is limited by background and is about one order of magnitude higher than predicted by Rule 07. The experimental data given for HgCdTe photodiodes in Teledyne Judson and VIGO catalogues are more than one order of magnitude below background flux limitation for the *f*/3 optics.

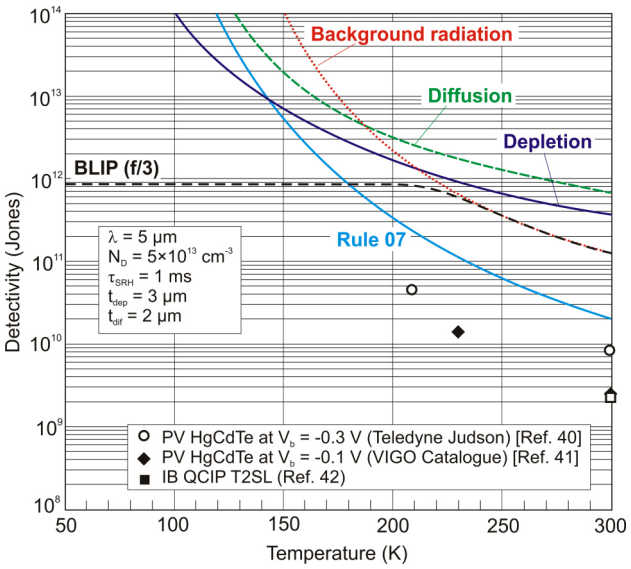

Fig. 9. Diffusion and depletion current components *vs*. temperature for MWIR P-i-N photodiode with the value of τ_{SRH} = 1 ms and absorber doping level of 5×10^{13} cm^{-3}. The thickness of active region is t = 5 μm and consists of t_{dif} = 2 μm and t_{dep} = 3 μm. The experimental data are taken with different sources as marked. PC – photo-conductor, PV – photodiode, IB QCIP - interband quan-tum cascade infrared photodetector.

3.3 *Detectivity: HgCdTe photodiode* vs. *2D material photodetectors*

Figure 10 presents detectivity curves gathered from literature for HOT MWIR and LWIR photodetectors - both for com mercially available detectors (PV Si and InGaAs, PC PbS and PbSe, HgCdTe photodiodes), as well as for 2D material photodetectors. Also, Johnson-noise limited detectivity values of new emerging IB QCIPs fabricated using InAs/GaSb T2SL absorbers are marked. All experimental data gathered in Fig. 10 indicates on sub- BLIP photodetectors performance. HgCdTe is currently most commonly used variable gap semiconductor for IR photodetectors, including operation at HOT conditions. It can be seen that the performance of HgCdTe photodiodes and T2SL IB QCIB are comparable, but due to strong covalent bonding of III - V compounds, IB QCIPs can operate at temperatures up to 400° C, what is not possible to reach for the HgCdTe counterpart due to strong interdiffusion processes.

In Fig. 10 there are also marked representative experimental data for 2D material single photodetectors operated in the infrared spectral range. The upper detectivity of Gr/FGr photodetector in MWIR is close to HgCdTe photodiodes. However, especially high detectivity (higher than for HgCdTe photodiodes) is demonstrated in Ref. 43 for black phosphorus arsenic (bPAs) photo-detectors and noble transition metal dichalcogenide photodetectors [44]. We can see that in the MWIR spectral range the performance of bPAs detectors outperform commercially available uncooled HgCdTe photodiodes, instead in LWIR, detectivity of noble transition metal dichalcogenide photodetectors is the best. Here it belongs to allude, that the serious drawback of black phosphorus is surface instable in ambient conditions what can considerably limit its prospective applications [48]. More promising there are stable noble TMD photodetectors like $PdSe_2/MoS_2$ heterojunction with record detectivity in the LWIR range at room temperature.

Figure 11 gathers the highest detectivity values published in literature for different types of single element 2D material photodetectors operated at room temperature. This fact should be clearly emphasised since detectivity data marked for commercial photodetectors is typical for pixels in infrared focal plane arrays. As is shown, the detectivity values for selected 2D material photodetectors are closed to data presented for commercial detectors (PV Si and Ge, PV InGaAs, PC PbS and PbSe, PV HgCdTe), and in the case of black phosphorus and noble transition metal dichalcogenide photodetectors are even higher. The enhanced sensitivity of 2D material photodetectors is introduced by bandgap engineering and photogating effect which degrade the electronic material properties including carrier mobility. In consequence, the layered-material photodectors are characterized by a limited linear dynamic range of operation and a slower response time in comparison with standard commercial photodetectors.

Figure 11 also directs on the fundamental indicator for future trend in development of HOT infrared photodetectors. At present stage of HgCdTe technology, the semiempirical rule Rule 07 is found not to fulfil primary expectations. It is shown that the detectivity of low-doping

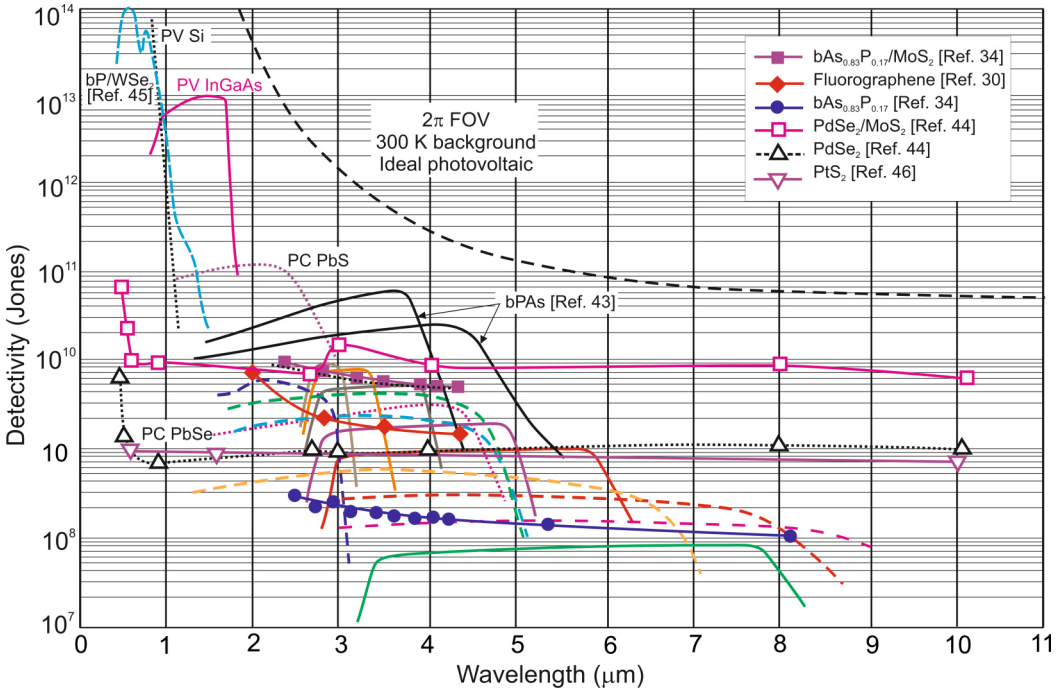

Fig. 10. Room-temperature spectral detectivity curves of the commercially available photodetectors [PV Si and InGaAs, PC PbS and PbSe, HgCdTe photodiodes (solid lines – Ref. 40)]. The experimental data for different types of 2D material photodetectors are included (Refs. 30,34,43-46). Also, spectral detectivity curves (dashed lines) of new emerging T2SL IB QCIPs are marked [47]. PC – photoconductor, PV – photodiode.

P-i-N HgCdTe (5×10^{13} cm^{-3}) photodiodes, operating at room-temperature in a spectral band above 3 μm, is limited by the background radiation (with D^* level above 10^{10} Jones, not limited by detector itself) and can be improved more than one order of magnitude in comparison with predicted by Rule 07. Between different material systems used in fabrication of HOT LWIR photodetectors, only HgCdTe ternary alloy can fulfil required expectations: low doping concentration – 10^{13} cm^{-3} and high SRH carrier lifetime – above 1 ms. In this context it will be rather difficult to rival 2D material photodetectors with HgCdTe photodiodes. The above estimates provide further encouragement for achieving low-cost and high performance MWIR and LWIR HgCdTe focal plane arrays operated in HOT conditions.

4. Conclusions

Discovery of graphene in 2004 gave a new impetus on technology developments and investigations of 2D layered materials. Their extraordinary and unusual electronic and optical properties make them promising candidates for infrared detectors. In spite of a spectacular demonstration of high detectivity like this achieved for black phosphorus [34] and noble transition metal dichalcogenide layered photodetectors [44], many challenges remain to be

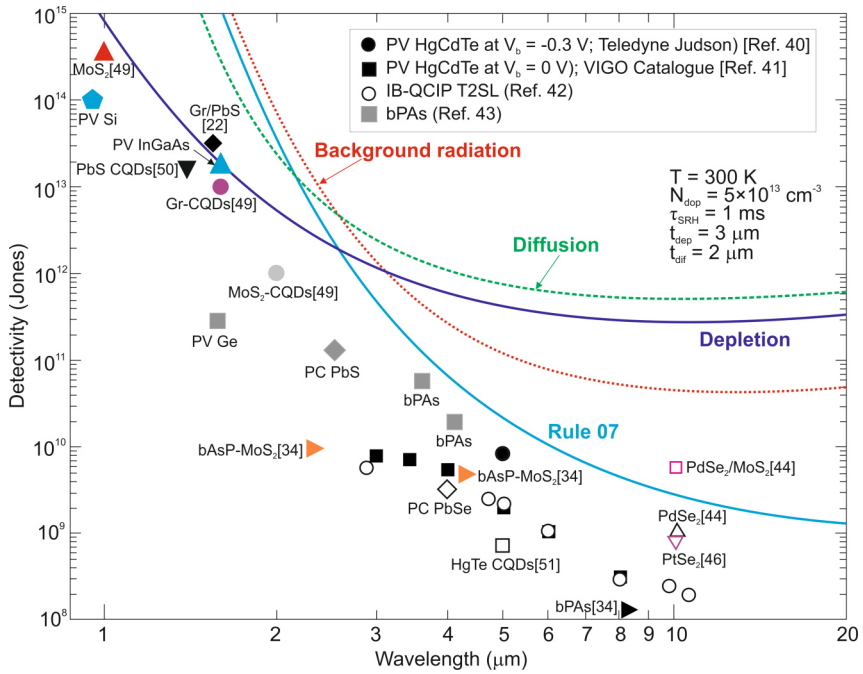

Fig. 11. Dependence of detectivity for the currently employed room-temperature operating HOT infrared photodetectors (PV Si and Ge, PV InGaAs, PC PbS and PbSe, PV HgCdTe), IB QCIP T2SLs, and different type of 2D material photodetectors. The experimental data are taken from literature as marked. The theoretical curves are calculated for P-i-N HOT HgCdTe photodiodes assuming the value of τ_{SRH} = 1 ms, the absorber doping level of 5×10^{13} cm^{-3} and the thickness of active region t = 5 μm. PC – photoconductor, PV – photodiode. The experimental data are taken from literature as marked [22,34,40-44,46,49-51].

introduced in order to exploit distinct advantages of these new materials. The prospect of commercialization of 2D material photodetectors depends on their large-scale integration with existing photonic and electronic platforms like CMOS technologies, high operability, spatial uniformity temporal stability, and affordability. Industry fabrication of devices is in the early stage of development and manufacturability.

In general, pristine narrow gap 2D materials are characterized by weak optical absorption and short carrier lifetime. Various ingenious approaches (electron trap layers, photogating effect with 2D material fast transfer channel) enhance sensitivity, however on the other side, degrade the electronic performance including carrier mobility. In this way high 2D material photodetector sensitivity collides with slow response time what limits its practical applications.

In spite of sixty years of HgCdTe ternary alloy system development history, its ultimate HOT performance limit has not been achieved. To achieve this goal, the doping concentration below 5×10^{13} cm^{-3} is required. This level of doping concentration has been recently demonstrated in fully depleted HgCdTe FPAs by Teledyne Technologies [21].

This paper has shown that the potential properties of HOT HgCdTe photodiodes operated in longer wavelength infrared range (above 3 μm) guarantee achieving more than order of magnitude higher detectivity (above 10^{10} Jones) in comparison with value predicted by Rule 07, and this detectivity is limited by background. In this context it is rather difficult to compete 2D material photodetectors with HgCdTe photodiodes.

Authors' statement

Research concept and design, A.R.; collection and/or assembly of data, A.R. and M.K.; data analysis and interpretation, A.R. and M.K.; writing the article, A.R.; critical revision of the article, P.M. and W.H.; final approval of article, P.M.

Acknowledgements

This work was supported by the funds granted to the Faculty of Advanced Technologies and Chemistry, Military University of Technology, within the subsidy for maintaining research potential in 2020, grant no. UGB763.

References

[1] Iwert, O. & Delabrea, B. The challenge of highly curved monolithic imaging detectors. *Proc. SPIE* **7742**, 774227-1-9 (2010).

[2] Jeong, K.-H. Kim, J. & Lee, L. P. Biologically inspired artificial compound eyes. *Science (80-.).* **312**, 557–561 (2006).

[3] Song, Y. M., Xie, Y., Malyarchuk, V., Xiao, J., Jung, I., Choi, K.-J., Liu, Z., Park, H., Lu, C., Kim, R. H., Li, R., Crozier, K. B., Huang, Y. & Rogers, J. A. Digital cameras with designs inspired by the arthropod eye. *Nature* **497**, 95–99 (2013).

[4] Tang, X., Ackerman, M. M. & Guyot-Sionnest, P. Colloidal quantum dots based infrared electronic eyes for multispectral imaging. *Proc. SPIE* **11088**, 1108803-1-7 (2019).

[5] Lu, Q., Liu, W. & Wang, X. 2-D material-based photodetectors on flexible substrates. in *Inorganic Flexible Optoelectronics: Materials and Applications* (eds. Ma, Z. & Liu, D.) 117-142 (Wiley-VCH Verlag, 20 19).

[6] Novoselov, K. S., Geim, A. K., Morozov, S. V., Jiang, D., Zhang, Y., Dubonos, S. V., Grigorieva, I. V. & Firsov, A. A. Electric field effect in atomically thin carbon films. *Science* **306**, 666-669 (2004).

[7] Mounet, N., Gibertini, M., Schwaller, P., Merkys, A., Castelli, I. E., Cepellotti, A., Pizzi, G. & Marzari, N. Two-dimensional materials from high-throughput computational exfoliation of experimentally known compounds. *Nat. Nanotechnol.***13**, 246-252 (2018).

[8] Rogalski, A. Graphene-based materials in the infrared and terahertz detector families: a tutorial. *Adv. Opt. Photonics* **11**, 314 (2019).

[9] Rogalski, A., Kopytko, M. & Martyniuk, P. Two-dimensional infrared and terahertz detectors: Outlook and status. *Appl. Phys. Rev.* **6**, 021316 (2019).

[10] Tennant, W. E., Lee, D., Zandian, M., Piquette, E. & Carmody, M. MBE HgCdTe technology: A very general solution to IR detection, descibrd by 'Rule 07', a very convenient heuristic. *J. Electron. Mater.* **37**, 1406-1410 (2008).

[11] Lee, D., Carmody, M., Piquette, E., Dreiske, P., Chen, A., Yulius, A., Edwall, D., Bhargava, S., Zandian, M., & Tennant, W.E. High-operating temperature HgCdTe: A vision for the near future. *J. Electron. Mater.* **45**, 4587-4595 (2016).

[12] Rogalski, A., Kopytko, M. & Martyniuk, P. Performance prediction of p-i-n HgCdTe long-wavelength infrared HOT photodiodes. *Appl. Opt.* **57**, D11 (2018).

[13] Elliott, C. T., Gordon, N. T. & White, A. M. Towards background-limited, room-temperature, infrared photon detectors in the 3–13 μm wavelength range. *Appl. Phys. Lett.* **74**, 2881–2883 (1999).

[14] Robinson, J., Kinch, M., Marquis, M., Littlejohn, D. & Jeppson, K. Case for small pixels: system perspective and FPA challenge. *Proc. SPIE* **9100**, 91000I-1-10 (2014).

[15] Rogalski, A., Martyniuk, P. & Kopytko, M. Challenges of small-pixel infrared detectors: a review. *Reports Prog. Phys.* **79**, 046501 (2016).

[16] Holst G. C. & Lomheim, T. C. CMOS/CCD Sensors and Camera Systems. (JCD Publishing and SPIE Press, Winter Park, 2007).

[17] Kinch, M.A. State-of-the-Art Infrared Detector Technology. (SPIE Press, Bellingham, 2014).

[18] Holst, G. C. & Driggers, R. G. Small detectors in infrared system design. *Opt. Eng.* **51**, 096401-1-10 (2012).

[19] Kinch, M. S., Aqariden, F., Chandra, D., Liao, P.-K., Schaake, H. F. & Shih, H. D. Minority carrier lifetime in p-HgCdTe. *J. Electron. Mater.* **34**, 880–884 (2005).

[20] Gravrand, O., Rothman, J., Delacourt, B., Boulard, F., Lobre, C., Ballet, P. H., Santailler, J. L., Cervera, C., Brellier, D., Pere-Laperne, N., Destefanis, V. & Kerlain, A. Shockley-Read-Hall lifetime study and implication in HgCdTe photodiodes for IR detection. *J. Electron. Mater.* **47**, 5680-5690 (2018).

[21] Lee, D., Dreiske, P., Ellsworth, J., Cottier, R., Chen, A., Tallarico, S., Barr, H., Tcheou, H., Yulius, A., Carmody, M., Piquette, E., Zandian, M. & Dougla, S. Performance of MWIR and LWIR fully-depleted HgCdTe FPAs. (Extended Abstracts. The 2019 U.S. Workshop on the Physics and Chemistry of II-VI Materials, 189-190, 2019).

[22] Konstantatos, G., Badioli, M., Gaudreau, L., Osmond, J. Bernechea, M., Garcia de Arquer, F. P., Gatti, F. & Koppens F. H. L. Hybrid graphene-quantum dot phototransistors with ultrahigh gain. *Nat. Nanotechnol.* **7**, 363–368 (2012).

[23] Wang, P., Xia, H., Li, Q., Wang, F., Zhang, L., Li, T., Martyniuk, P., Rogalski, A. & Hu, W. Sensing infrared photons at room temperature: from bulk materials to atomic layers. *Small* **46**, 1904396 (2019).

[24] Currie, M. Applications of graphene to photonics. (NRL/MR/5650-14-9550, 2014).

[25] Furchi, M., Urich, A., Pospischil, A., Lilley, G., Unterrainer, K., Detz, H., Klang, P., Andrews, A. M., Schrenk, W., Strasser, G. & Mueller, T. Microcavity-integrated graphene photodetector. *Nano Lett.* **12**, 2773–2777 (2012).

[26] Ferreira, A., Peres, N. M. R., Ribeiro, R. M. & Stauber, T. Graphene-based photodetector with two cavities. *Phys. Rev. B* **85**, 115438 (2012).

[27] Zhang, Y., Liu, T., Meng, B., Li, X., Liang, G., Hu, X., & Wang, Q. J. Broadband high photoresponse from pure monolayer graphene photodetector. *Nat. Commun.* **4**, 1811 (2013).

[28] Gan, X., Shiue, R.-J., Yuanda, G., Meric, I., Heinz, T.F., Shepard, K., Hone, J., Assefa S. & Englund, D. Chip-integrated ultrafast

graphene photodetector with high responsivity. *Nat. Photonics* **7**, 883–887 (2013).

[29] Chang, P.-H., Liu, S.-Y., Lan, Y-B., Tsai, Y.-C., You, X.-Q., Li, C.-S., Huang, K.-Y., Chou, A.-S., Cheng, T.-C., Wang, J.-K. & Wu, C.-I. Ultrahigh responsivity and detectivity graphene–perovskite hybrid phototransistors by sequential vapor deposition. *Sci. Rep.* **7**, 46281 (2017).

[30] Du, S., Lu, W., Ali, A., Zhao, P., Shehzad, K., Guo, H., Ma, L., Liu, X., Pi, X., Wang, P., Fang, H., Xu, Z., Gao, C., Dan, Y., Tan, P., Wang, H., Lin, C.-T., Yang, J., Dong, S., Cheng, Z., Li, E., Yin, W., Luo, J., Yu, B., Hasan, T., Xu, Y., Hu, W. & Duan, X. A broadband fluorographene photodetector. *Adv. Mater*. **29**, 1700463 (2017).

[31] Chen, Z., Li, X., Wang, J., Tao, L., Long, M., Liang, S.-J., Ang, L.K., Shu, C., Tsang, H. K. & Xu, J.-B. Synergistic effects of plasmonics and electron trapping in graphene short-wave infrared photodetectors with ultrahigh responsivity. *ACS Nano* **11**, 430−437 (2017).

[32] Cakmakyapan, S., Lu, P. K., Navabi, A. & Jarrahi, M. Gold-patched graphene nano-stripes for high-responsivity and ultrafast photodetection from the visible to infrared regime. *Light Sci. Appl.* **7**, 20 (2018).

[33] Wang, F., Wang, Z., Yin, L., Cheng, R., Wang, J., Wen, Y., Shifa, T. A., Wang, F., Zhang, Y., Zhan, X., & He, J. 2D library beyond graphene and transition metal dichalcogenides: a focus on photodetection. *Chem. Soc. Rev.* **47**, 6296–6341 (2018).

[34] Long, M., Gao, A., Wang, P., Xia, H., Ott, C., Pan, C., Fu, Y., Liu, E., Chen, X., Lu, W., Nilges, T., Xu, J., Wang, X., Hu, W. & Miao, F. Room temperature high-detectivity mid-infrared photodetectors based on black arsenic phosphorus. *Sci. Adv.* **3**, e1700589 (2017).

[35] Buscema, M., Islan, J. O., Groenendijk, D. J., Blanter, S. I., Steele, G. A., van der Zant, H. S. J. & Castellanos-Gomez, A."Photocurrent generation with two-dimensional van der Waals semiconductor. *Chem. Soc. Rev.* **44**, 3691-3718 (2015).

[36] Wang, J., Fang, H., Wang, X., Chen, X., Lu, W. & Hu, W. Recent progress on localized field enhanced two-dimensional material photodetectors from ultraviolet-visible to infrared. *Small* **13**, 1700894 (2017).

[37] Long, M., Wang, P., Fang, H. & Hu, W. Progress, challenges, and opportunities for 2D material based photodetectors. *Adv. Funct. Mater*. **29**, 1803807 (2018).

[38] Ashley, T. & Elliott, C. T. Non-equilibrium mode of operation for infrared detection. *Electron. Lett.* **21**, 451–452 (1985).

[39] Elliott, C. T. Non-equilibrium mode of operation of narrow-gap semiconductor devices. *Semicond. Sci. Technol.* **5**, S30–7 (1990).

[40] HOT MCT Detectors, http://www.teledynejudson.com/

[41] https://vigo.com.pl/wp-content/uploads/2017/06/VIGO-Catalogue.pdf

[42] Huang, W., Rassela, S. M. S., Li, L., Massengale, J.A., Yang, R.Q., Mishima, T. D. & Santos, M.B. A unified figure of merit for interband and intersubband cascade devices. *Infrared Phys. Technol*. **96**, 298-301 (2019)

[43] Amani, M., Regan, E., Bullock, J., Ahn, G. H. & Javey, A. Mid-wave infrared photoconductors based on black phosphorus-arsenic alloys. *ACS Nano* **11**, 11724–11731 (2017).

[44] Long, M., Wang, Y., Wang, P., Zhou, X., Xia, H., Luo, C., Huang, S., Zhang, G., Yan, H., Fan, Z., Wu, X., Chen, X., Lu, W. & Hu, W. Palladium diselenide long-wavelength infrared photodetector with high sensitivity and stability. *ACS Nano* **13**, 2511−2519 (2019).

[45] Ye, L., Wang, P., Luo, W., Gong, F., Liao, L., Liu, T., Tong, L., Zang, J., Xu, J. & Hu, W. Highly polarization sensitive infrared photodetector based on black phosphorus-on-WSe_2 photogate vertical heterostructure. *Nano Energy* **37**, 53-60 (2017)

[46] Yu, X., Yu, P., Wu, D., Singh, B., Zeng, Q., Lin, H., Zhou, W., Lin, J., Suenaga, K., Liu, Z. & Wang, Q. J. Atomically thin noble metal dichalcogenide: a broadband mid-infrared semiconductor. *Nat. Commun.* **9**, 1545 (2018).

[47] Rogalski, A., Martyniuk, P. & Kopytko, M. Type-II superlattice photodetectors versus HgCdTe photodiodes. *Prog. Quantum Electron.* **68**, 100228 (2019).

[48] Wang, X., Sun, Y. & Liu, K. Chemical and structural stability of 2D layered materials. *2D Mater.* **6**, 042001 (2019).

[49] Konstantatos, G. Current status and technological prospect of photodetectors based on two-dimensional materials. *Nat. Commun.* **9**, 5266 (2018).

[50] Konstantatos, G. & Sargent, E. H. Solution-processed quantum dot photodetectors. *Proc. IEEE* **97**, 1666-1683 (2009).

[51] Guyot-Sionnest, P., Ackerman, M. M. & Tang, X. Colloidal quantum dots for infrared detection beyond silicon. *J. Chem. Phys.* **151**, 060901 (2019).